

Accepted Manuscript

Methylpyrrole inhibitors of BET bromodomains

Lisa A. Hasvold, George S. Sheppard, Le Wang, Steven D. Fidanze, Dachun Liu, John K. Pratt, Robert A. Mantei, Carol K. Wada, Robbert Hubbard, Yu Shen, Xiaoyu Lin, Xiaoli Huang, Scott E. Warder, Denise Wilcox, Leiming Li, F. Greg Buchanan, Lauren Smithee, Daniel H. Albert, Terrance J. Magoc, Chang H. Park, Andrew M. Petros, Sanjay C. Panchal, Chaohong Sun, Peter Kovar, Nirupama B. Soni, Steven W. Elmore, Warren M. Kati, Keith F. McDaniel

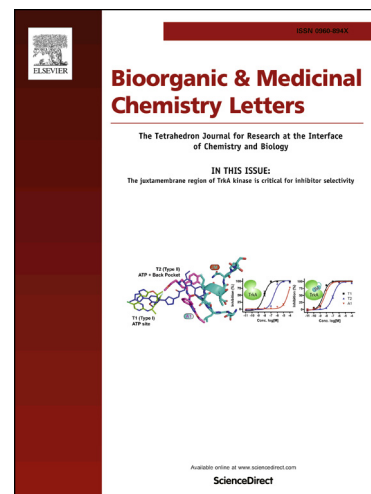
PII: S0960-894X(17)30200-7
DOI: <http://dx.doi.org/10.1016/j.bmcl.2017.02.057>
Reference: BMCL 24729

To appear in: *Bioorganic & Medicinal Chemistry Letters*

Received Date: 5 January 2017
Revised Date: 17 February 2017
Accepted Date: 23 February 2017

Please cite this article as: Hasvold, L.A., Sheppard, G.S., Wang, L., Fidanze, S.D., Liu, D., Pratt, J.K., Mantei, R.A., Wada, C.K., Hubbard, R., Shen, Y., Lin, X., Huang, X., Warder, S.E., Wilcox, D., Li, L., Buchanan, F.G., Smithee, L., Albert, D.H., Magoc, T.J., Park, C.H., Petros, A.M., Panchal, S.C., Sun, C., Kovar, P., Soni, N.B., Elmore, S.W., Kati, W.M., McDaniel, K.F., Methylpyrrole inhibitors of BET bromodomains, *Bioorganic & Medicinal Chemistry Letters* (2017), doi: <http://dx.doi.org/10.1016/j.bmcl.2017.02.057>

This is a PDF file of an unedited manuscript that has been accepted for publication. As a service to our customers we are providing this early version of the manuscript. The manuscript will undergo copyediting, typesetting, and review of the resulting proof before it is published in its final form. Please note that during the production process errors may be discovered which could affect the content, and all legal disclaimers that apply to the journal pertain.

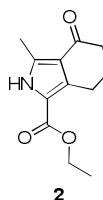
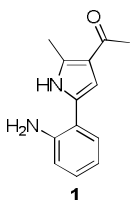


Graphical Abstract

**Methylpyrrole inhibitors of BET
bromodomains**

Leave this area blank for abstract info.

Lisa A. Hasvold*, George S. Sheppard*, Le Wang, Steven D. Fidanze, Dachun Liu, John K. Pratt, Robert A. Mantei, Carol K. Wada, Robert Hubbard, Yu Shen, Xiaoyu Lin, Xiaoli Huang, Scott E. Warder, Denise Wilcox, Leiming Li, F. Greg Buchanan, Lauren Smithee, Daniel H. Albert, Terrance J. Magoc, Chang H. Park, Andrew M. Petros, Sanjay C. Panchal, Chaohong Sun, Peter Kovar, Nirupama B. Soni, Steven W. Elmore, Warren M. Kati and Keith F. McDaniel





Methylpyrrole inhibitors of BET bromodomains

Lisa A. Hasvold^{a*}, George S. Sheppard^{a*}, Le Wang^a, Steven D. Fidanze^a, Dachun Liu^a, John K. Pratt^a, Robert A. Mantel^a, Carol K. Wada^a, Robbert Hubbard^b, Yu Shen^a, Xiaoyu Lin^a, Xiaoli Huang^a, Scott E. Warder^a, Denise Wilcox^a, Leiming Li^a, F. Greg Buchanan^a, Lauren Smithee^b, Daniel H. Albert^a, Terrance J. Magoc^b, Chang H. Park^a, Andrew M. Petros^a, Sanjay C. Panchal^a, Chaohong Sun^a, Peter Kovar^a, Nirupama B. Soni^a, Steven W. Elmore^a, Warren M. Kati^a and Keith F. McDaniel^a

^aAbbVie Inc., Oncology Discovery, 1 North Waukegan Rd., North Chicago, IL 60064, USA

^bFormer AbbVie employee

ARTICLE INFO

Article history:

Received
Revised
Accepted
Available online

ABSTRACT

An NMR fragment screen for binders to the bromodomains of BRD4 identified 2-methyl-3-ketopyrroles **1** and **2**. Elaboration of these fragments guided by structure-based design provided lead molecules with significant activity in a mouse tumor model. Further modifications to the methylpyrrole core provided compounds with improved properties and enhanced activity in a mouse model of multiple myeloma.

2009 Elsevier Ltd. All rights reserved.

Keywords:

BET proteins
Bromodomain
Fragment Screening

The BET (Bromodomain and Extraterminal) family of proteins, consisting of BRD2, BRD3, BRD4 and BRDT, has emerged as a promising epigenetic target for drug discovery.¹ These proteins act as epigenetic 'readers' that recognize acetylated lysines on the *N*-terminal tails of histones and recruit transcription factors to chromatin. This recognition occurs through interaction with a structural motif called a bromodomain,² with each BET protein containing two bromodomains. Many of the interacting transcription factors and their target genes are known to play roles in the pathogenesis of cancer and inflammation. Accordingly, small molecules which bind to the bromodomains present in the BET family proteins have shown activity in a wide range of preclinical disease models, and multiple compounds have advanced into clinical trials for the treatment of cancers.³

In an effort to discover novel BET bromodomain inhibitors, we undertook a fragment-based approach using NMR screening⁴ with a TR-FRET competitive binding assay to confirm binding. A number of structural types which had not been previously reported to bind to bromodomains were identified.⁵ Two such fragment hits were the 2-methyl-3-keto pyrroles **1** and **2**, which showed a large degree of spectral perturbation,⁴ moderate binding affinities and high binding efficiency indices (BEI)⁶ (Figure 1).

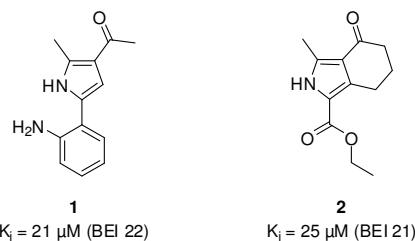


Figure 1. NMR fragment hits **1** and **2**.

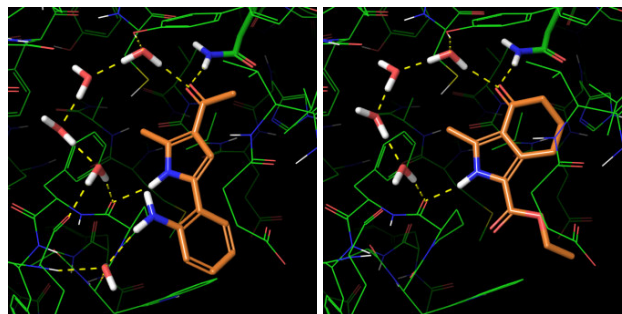


Figure 2. X-ray co-crystal structures of fragments **1** and **2** in the BRD4 BDII protein. Residues Pro378 and Val379 are not displayed for clarity. Dotted lines represent H-bonds predicted by Schrödinger Maestro.

The X-ray co-crystal structures of compounds **1** (PDB code: 5UEV) and **2** (PDB code: 5UEP) (Figure 2) with bromodomain II of BRD4 revealed several key interactions between the ligands

and the protein which consists of four α -helices (α_Z , α_A , α_B and α_C) and two loops, one linking helices α_Z and α_A (ZA loop) and a second linking helices α_B and α_C (BC loop).⁷ The compounds bind in the acetyl lysine recognition site of the bromodomain, with the 3-keto functionality of both compounds accepting a hydrogen bond from the Asn433 sidechain amide. The 2-methyl group on each pyrrole ring resides in an ordered water network forming an amphoteric pocket. In addition to the Asn433 interaction, the 3-keto functionality of each compound also hydrogen bonds with a nearby water molecule in the amphoteric pocket. In each structure the pyrrole NH interacts with the Pro375 carbonyl group. For compound **1**, a water molecule bridges between the aniline and the amide backbone of the ZA loop.

Co-crystal structures of related analogs provided additional insight into the binding of the fragments. Compounds **3** and **4**, containing a primary amide in place of the methyl ketone moiety in **1**, displayed similar binding affinity (Figure 3); however, a second hydrogen bond between the amide and the Asn433 residue of the BRD4 BDII protein was observed for compound **3** (PDB code: 5UET) (Figure 4). Replacing the ester moiety of compound **2** with the 2-aniline moiety (compound **5**) provided a small improvement in activity (Figure 3).

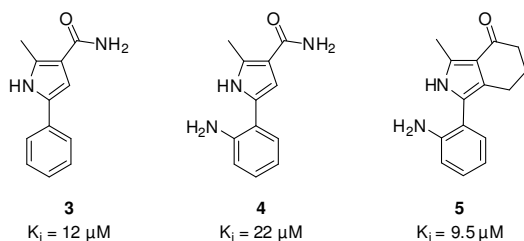


Figure 3. Compounds **3**, **4** and **5**.

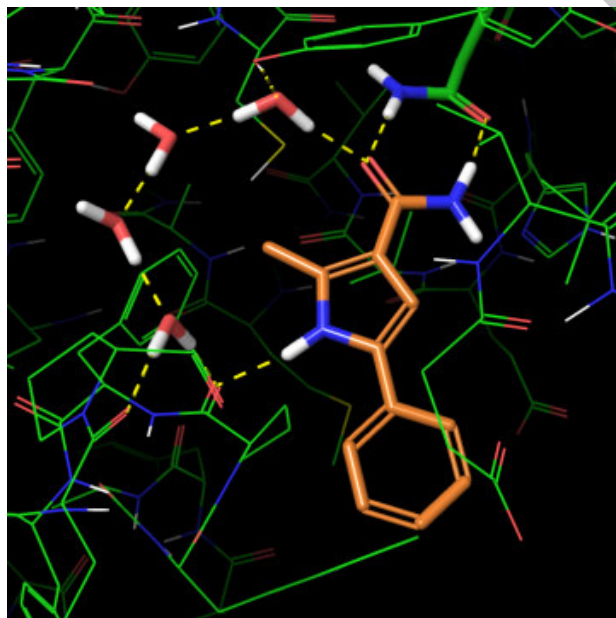


Figure 4. X-ray co-crystal structure of compound **3** in the BRD4 BDII protein. Residues Pro378 and Val379 are not displayed for clarity. Dotted lines represent H-bonds predicted by Schrödinger Maestro.

An overlay of the X-ray co-crystal structures of compound **1** and known BET inhibitor **6** (MS417)⁸ (PDB code: 5UEU) shown in Figure 5 revealed additional exploitable binding sites within the protein, such as the WPF shelf, which is comprised of residues W374, P375 and F376.⁹ The WPF shelf is occupied by the 4-chlorophenyl moiety of compound **6**, but is not occupied by compound **1**. Occupation of the WPF shelf is reported to provide

selectivity versus non-BET bromodomains.¹⁰ Additionally, there is an extended cleft between the ZA loop and the adjacent helix that neither compound fully occupies. By placing substituents on the phenyl ring at the appropriate positions with vectors directed toward these unoccupied regions of the protein, it may be possible to gain additional interactions with the protein and improve potency. Several compounds related to fragments **1** and **2** were prepared to investigate these areas of the protein (Table 1).

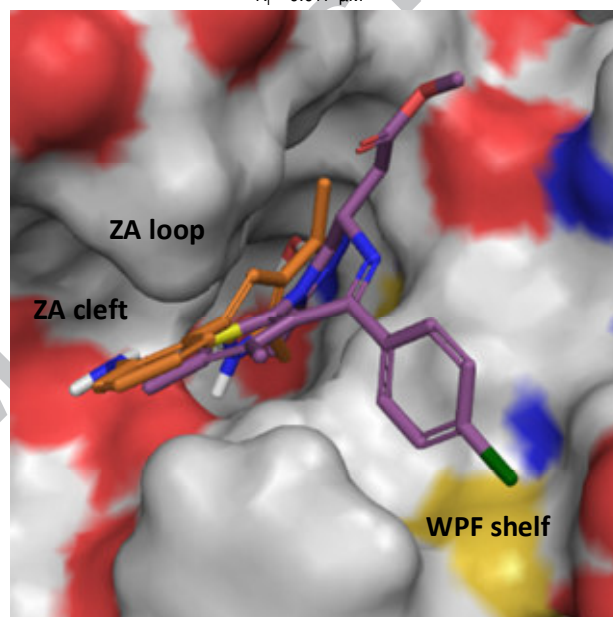
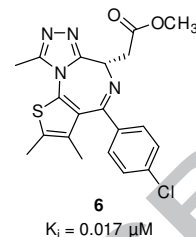


Figure 5. X-ray co-crystal structure overlay of fragment **1** (orange) and compound **6** (MS417) in the BRD4 BDII protein.

Compounds were evaluated using a binding assay and two cellular assays. Binding to a construct containing both bromodomains of BRD4 (K57-K550) was determined using a TR-FRET assay as described in the supplementary material. Binding determinations to other bromodomains of the BET family showed no meaningful selectivity within the family; these data are reported for key compounds **15**, **25** and **38** in the supplementary material. Single concentration screening experiments against selected non-BET bromodomains are also reported for **15**, **25** and **38** in the supplementary material and indicate low affinity for most of the non-BET bromodomains examined. Cellular proliferation was measured using the triple negative breast cancer cell line MX-1 (ATCC) in a 3-day proliferation assay using the Cell Titer Glo assay kit (Promega). Target engagement in cells was measured with a luciferase reporter assay based on the contribution of BRD4 to human papilloma virus (HPV) E2-mediated transcriptional repression, where BRD4 is part of the HPV long control region (LCR) promoter repression complex with E2 and EP400.¹¹ An H1299-derived cell line was generated with a stably integrated E2 expression cassette and an HPV-LCR-driven luciferase reporter. A luciferase signal occurs only when a BET inhibitor blocks BRD4, thus providing a measure of target engagement. Good

correlation was observed between the two cellular assays, an indication that cell killing is due to target engagement.

To access the WPF shelf region, phenylamino and phenoxy groups were placed on the phenyl ring of compound **3**. It can be seen in Table 1 that a significant gain in binding activity was observed upon addition of phenylamino (compound **7**, 50-fold) or phenoxy substituents (compound **8**, 80-fold; compound **9**, 50-fold). The phenoxy substituents provided greater cellular potency in both the MX-1 and luciferase target engagement assays than the phenylamino moiety. The X-ray co-crystal structure of compound **9** (PDB code: 5UES) confirmed that the phenoxy group occupies the WPF shelf. It also indicates retention of the bidentate interaction between the primary amide and Asn433, the pyrrole NH interaction with Pro375 and the placement of the 2-methyl group among the waters in the amphoteric pocket (Figure 6).

In an effort to further enhance potency by reestablishing the aniline interactions with Pro375 and the amide backbone of the ZA loop, compound **10** which incorporates both the 2-amino and 6-phenoxy moieties was examined. This combination proved to be less active in the TR-FRET assay and both cellular assays compared to compound **8**. The amino moiety was then moved to the adjacent carbon, situating it para to the phenoxy moiety to provide a different vector for access to the ZA loop and adjacent cleft. Some activity was regained by the repositioning of the amine (compound **11**) and with incorporation of the methanesulfonamide moiety (compound **12**), but neither compound surpassed the potency of compound **8** with the single phenoxy substituent.

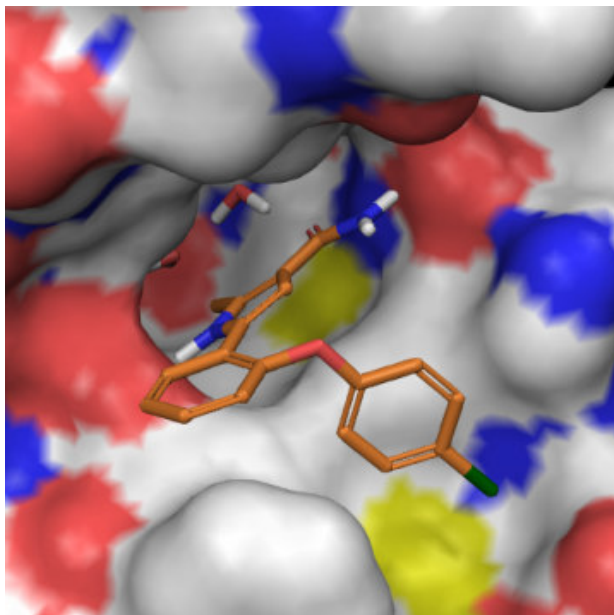


Figure 6. X-ray co-crystal structure of compound **9** in the BRD4 BDII protein.

Concurrently, similar substitutions on compound **5** were investigated. Similar to the potency gains observed with the fragment **1** structure, a greater than 20-fold gain in TR-FRET activity was obtained by replacement of amino with phenoxy on the compound **5** isoindolone structure (compound **13**). Cellular potency was substantially improved as well. In this case, a modest improvement in binding affinity was observed upon the addition of an amino group para to the phenoxy moiety (compound **14**) and an even larger 13-fold improvement in binding affinity was obtained when the methanesulfonamide moiety was added (compound **15**). Together these changes combined to provide an overall 760-fold gain in TR-FRET

binding activity for compound **15** compared to fragment **2**. Sizable improvements in activity were also achieved in both the cellular proliferation and luciferase reporter assays. Simple ester (compound **16**) and amide (compound **17**) moieties were also investigated at the same position. The methyl ester showed decreased TR-FRET activity compared to the sulfonamide moiety (91 nM vs. 33 nM), and an even more significant loss of TR-FRET activity was observed with the ethyl amide moiety (250 nM vs. 33 nM). Cellular potency also declined for both the methyl ester and ethyl amide compounds.

A co-crystal structure of compound **15** (PDB code: 5UER) bound to BRD4 BDII (Figure 7) was also obtained. As with compound **9**, the phenoxy group resides in the WPF pocket. An additional interaction was also achieved with one oxygen atom of the sulfonamide group being hydrogen bonded to the Asp381 backbone amide of the ZA loop. Surprisingly, in the fully elaborated molecule **15**, the isoindolone ring system was rotated compared to the X-ray co-crystal structure observed for fragment **2**. The rotated ring system retains the interaction between the isoindolone carbonyl group and Asn433. However, the methylene groups alpha and beta to the carbonyl group now occupy nearly the same space in the amphoteric pocket that the methyl group on the pyrrole ring occupied in all of the previously obtained X-ray co-crystal structures for the 2-methyl-3-keto pyrroles **1** and **2** and analogs containing those cores. An overlay of compounds **2** and **15** shown in Figure 8 illustrates how these compounds occupy the BRD4 BDII protein relative to each other.

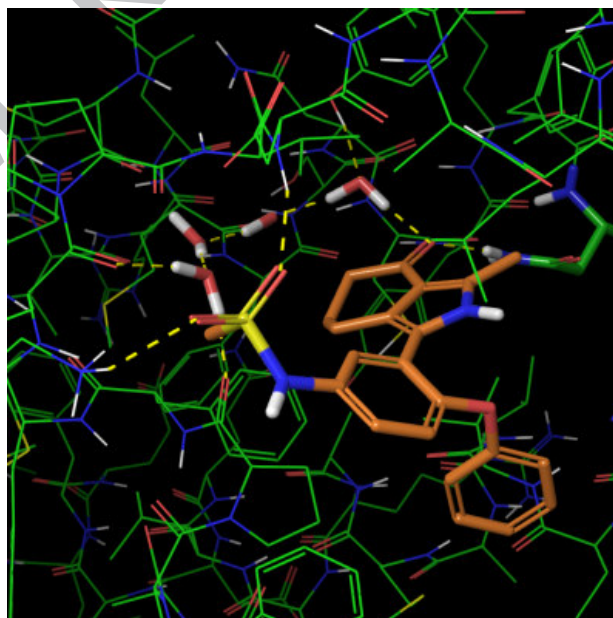


Figure 7. X-ray co-crystal structure of compound **15** in the BRD4 BDII protein. Dotted lines represent H-bonds predicted by Schrödinger Maestro.

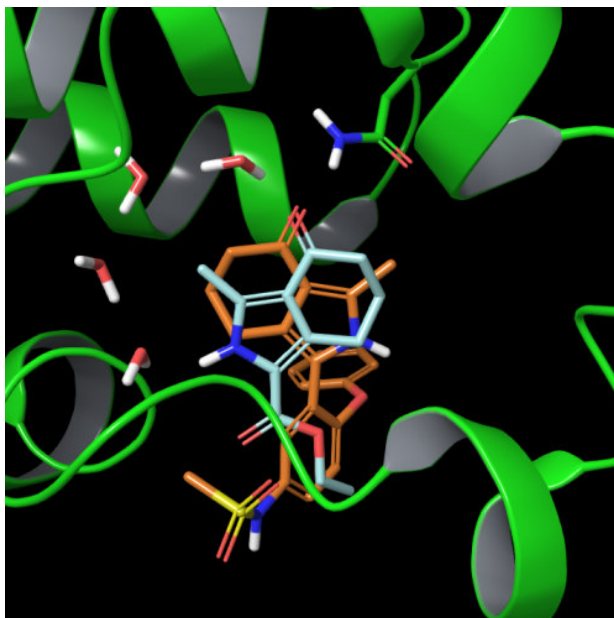


Figure 8. Overlay of X-ray co-crystal structures of **2** (blue) and **15** (orange) in the BRD4 BDII protein.

Among these early compounds, compound **15** stood out as having superior activity both in the TR-FRET binding assay and in the cellular assays. Mouse pharmacokinetic information for compound **15** is reported in Table 2. Compound **15** demonstrated high unbound i.v. clearance at 84 L/hr/kg and low unbound oral AUC of 0.09 $\mu\text{M}\cdot\text{hr}$ with 30% oral bioavailability. Though improvement in pharmacokinetics would be necessary, exposure was sufficient to take compound **15** forward into a xenograft tumor model for proof of concept studies.

Prior to the initiation of the xenograft model, a study to determine the maximum tolerated dose (MTD) indicated that compound **15** was well-tolerated at 100 mg per kg per day (mkd). Using this as a guide for dose selection, compound **15** was then evaluated in an OPM-2 mouse xenograft model of multiple myeloma dosed orally once a day (QD) at 100 mkd or twice a day (BID; 50 mkd x 2) over 14 days (Figure 9). Administration of the same total dose in a twice daily fashion provided improved tumor growth inhibition (TGI) of 73% compared to 53% TGI observed for daily QD dosing during the treatment period, due to longer coverage of the target. Both dosing regimens were well-tolerated. The moderate TGI observed confirmed the use of pyrrole-based BET inhibitors as possible cancer therapeutics and prompted further optimization of these cores to discover BET inhibitors with improved potency and ADME properties.

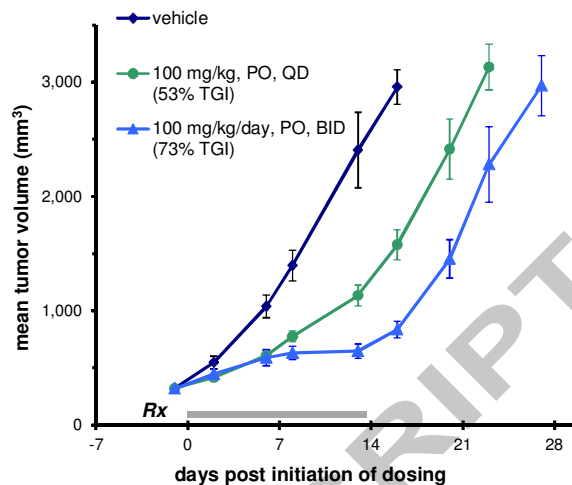
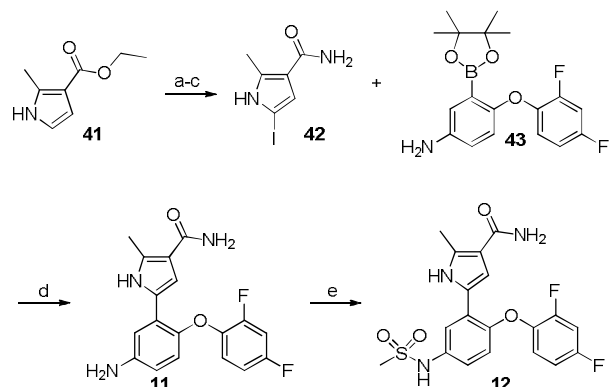


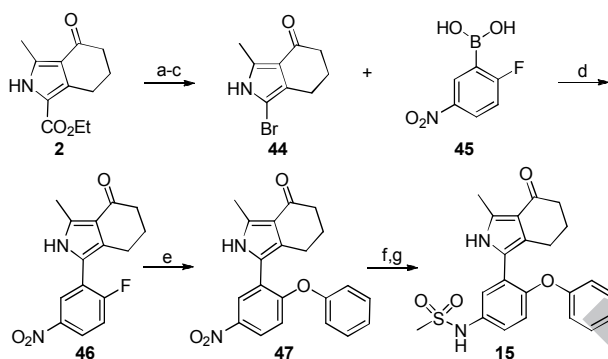
Figure 9. Tumor growth inhibition data for compound **15** in an OPM-2 xenograft model of multiple myeloma. Values represent mean \pm SE (n = 10 per group).

A metabolite identification study of compound **15** in both mouse and rat liver microsomes revealed the saturated isoindolone ring and the terminal phenoxy ring to be the primary sites of metabolism. As a possible means for improving activity and ADME properties, a variety of additional fused bicyclic pyrrole cores capable of producing a bidentate interaction with Asn433 similar to that observed with the amide-substituted monocyclic pyrrole core were prepared (Table 3). Cores III-VI introduced 1-2 nitrogen atoms into the fused ring and varied the ring saturation. For core VII, the nitrogen atom of core IV was moved over 1 atom, placing the methyl group on nitrogen instead of on carbon. In addition to the core changes, sulfonamide replacements that would potentially retain the ZA loop backbone interaction were also investigated. Additionally, 2,4-difluorophenoxy was investigated as a phenoxy replacement to block sites of metabolism and perhaps reduce the high unbound clearance observed in liver microsomes and in mouse pharmacokinetic experiments.

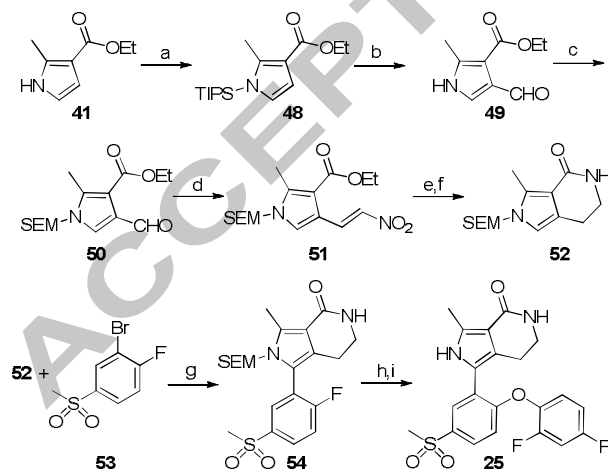
Prototypical synthetic schemes for the seven core types are shown in Schemes 1-7. Halogen substituted cores I, IV and V were prepared from the common starting material **41** and then coupled with the lower aryl piece via Suzuki-Miyaura cross coupling (Schemes 1, 4, and 5). Similarly, core VII was prepared through coupling of the iodoazaindole intermediate **67** (Scheme 7). Core II was prepared in a similar manner through elaboration of pyrrole ketone **2** (Scheme 2).¹² Alternatively, C-H activation of the pyrrole ring¹³ was used for the coupling of core III to the lower aryl piece (Scheme 3). Construction of the fused rings in cores III, IV and V utilized formylation at the 4-position of the pyrrole, achieved by temporary blocking of the 5-position through TIPS protection of the pyrrole nitrogen, followed by formation of the fused ring (Schemes 3, 4 and 5). In some cases, the phenoxy moiety was introduced after cross coupling through nucleophilic aromatic substitution. Core VI was assembled onto the lower aryl piece rather than coupling the completely formed core with the lower aryl piece (Scheme 6). Experimental procedures and spectral data for select compounds can be found in the supplementary material.



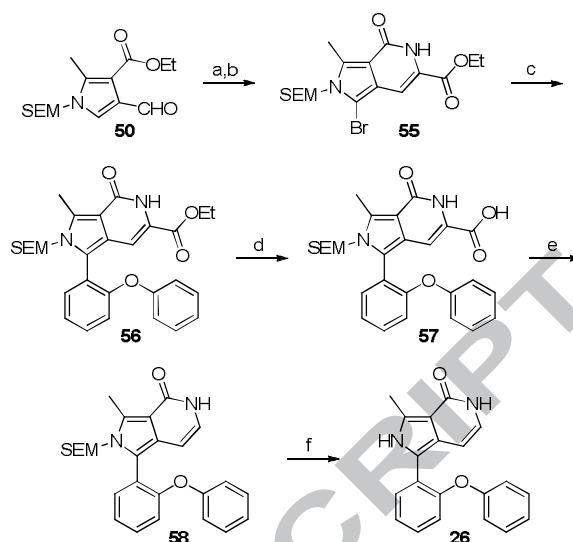
Scheme 1. Reagents and conditions: a) LiOH, 1,4-dioxane/H₂O, 73%; b) HATU, NH₃, DIPEA, 1,4-dioxane, DMF, 73%; c) NIS, THF, 71%; d) Pd₂(dba)₃, 1,3,5,7-tetramethyl-8-phenyl-2,4,6-trioxa-8-phosphaadamantane (PA-Ph), K₃PO₄, THF/H₂O, 60 °C, 37%; e) (i) CH₃SO₂Cl, DIPEA, DCM; (ii) NaOH (1 M aq.), THF, 50 °C, 70%.



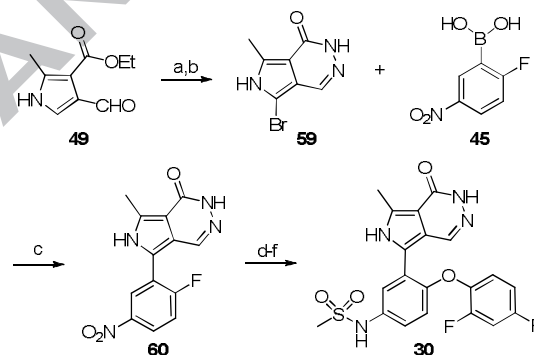
Scheme 2. Reagents and conditions: a) LiOH, THF/H₂O, 81%; b) HCl, EtOH/H₂O, heat, 62%; c) NBS, THF, -78 °C, 76%; d) Pd₂(dba)₃, PA-Ph, K₃PO₄, THF/H₂O, 60 °C, 71%; e) phenol, Cs₂CO₃, DMF, 110 °C, 85%; f) Fe, NH₄Cl, THF/EtOH/H₂O, reflux, 95%; g) (i) CH₃SO₂Cl, Et₃N, DCM; (ii) NaOH (1 M aq.), 1,4-dioxane, 50 °C, 86%.



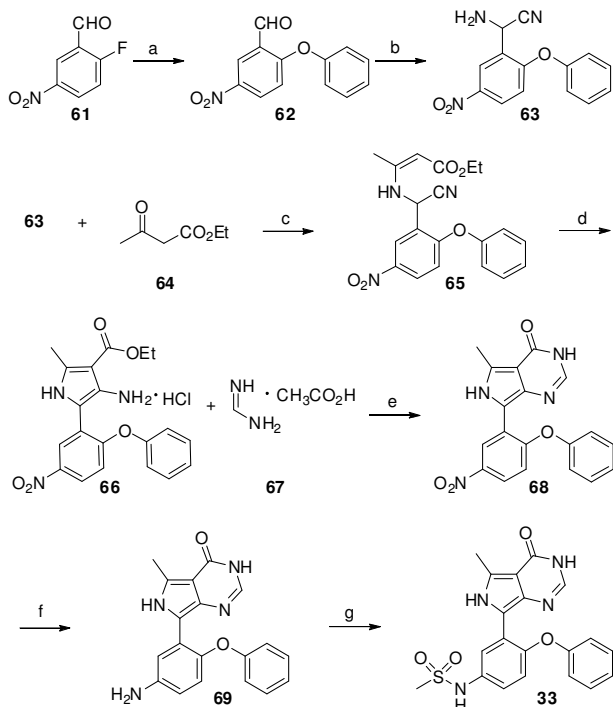
Scheme 3. Reagents and conditions: a) NaH, TIPSCl, THF, 88%; b) oxalyl chloride, DMF, DCM, 0 °C, 74%; c) NaH, SEMCl, THF, 89%; d) NH₄OAc, CH₃NO₂, 90 °C, 85-95%; e) H₂, washed Raney nickel, THF, 67-95%; f) LiOH, 95% EtOH, 120 °C, 60-77%; g) allyl PdCl dimer, KOAc, DMA, 130 °C, 38-43%; h) Cs₂CO₃, DMSO, 80 °C, 40%; i) (i) TFA; (ii) K₂CO₃, MeOH, 87%.



Scheme 4. Reagents and conditions: a) ethyl 2-isocyanoacetate, NaH, THF, 70 °C, 35%; b) NBS, THF, -78 °C, 78%; c) (2-phenoxyphenyl)boronic acid, Pd₂(dba)₃, PA-Ph, Na₂CO₃, 1,4-dioxane/H₂O, 60 °C, 63%; d) LiOH, THF/MeOH/H₂O, 50 °C, 98%; e) CuO, 1,10-phenanthroline, NMP/quinoline, 190 °C microwave; f) (i) TFA, RT; (ii) NaOAc, CH₃CN/H₂O, 50 °C, 15% e-f.



Scheme 5. Reagents and conditions: a) H₂NNH₂, H₂O, EtOH, 68%; b) NBS, DMF/THF, 54%; c) Pd₂(dba)₃, PA-Ph, K₃PO₄, THF/H₂O, 60 °C, 85%; d) 2,4-difluorophenol, Cs₂CO₃, DMF, 50 °C, 66%; e) H₂, Pd/C, EtOAc, 73%; f) (i) CH₃SO₂Cl, Et₃N, DCM; (ii) NaOH (1 M aq.), THF/1,4-dioxane, 75%.



Scheme 6. Reagents and conditions: a) phenol, K_2CO_3 , 1,4-dioxane, 70 °C, 99%; b) NaCN, NH_4Cl , NH_4OH , MeOH, 28%; c) *p*-TsOH, toluene, 80 °C, 99%; d) NaOEt, EtOH, 44%; e) EtOH, 80 °C, 38%; f) H_2 , Pd/C, MeOH, 78%; g) (i) CH_3SO_2Cl , Et_3N , DCM; (ii) K_2CO_3 , 1,4-dioxane, 50 °C, 56%.

Scheme 7. Reagents and conditions: a) NIS, DMF, 93%; b) NaH, CH_3I , DMF, 95%; c) $Pd_2(dba)_3$, PA-Ph, K_3PO_4 , THF/ H_2O , 60 °C, 88%; d) 2,4-difluorophenol, Cs_2CO_3 , DMSO, 110 °C, 94-99%; e) 4 M HCl, 1,4-dioxane, 71-87%.

Table 3 summarizes the activity and ADME data for the new cores compared to the original pyrrole and isoindolone cores. In general, for the compounds of Table 3 and others not shown, compounds based on cores III-V showed similar or diminished activity compared to the isoindolone core II-based compounds in both the TR-FRET binding assay and the cellular assays. It was also typically found for cores I-V and VII that replacement of - $NHSO_2Me$ with - SO_2Me and replacement of phenoxy with 2,4-difluorophenoxy resulted in a loss of activity in both the TR-FRET and cellular assays. Core VII, which differs from the other cores by the lack of hydrogen bonding capability between the pyrrole NH and Pro375 resulting from relocation of the pyrrole nitrogen, stood out with improved activity compared to the isoindolone core. It was also somewhat more active in the TR-FRET assay compared to core IV (compare compounds **26** and

34) consistent with the suggestion from the binding mode of **15** that the hydrogen bond between the pyrrole NH and Pro375 does not substantially contribute to the activity. For cores III, V and VI, analogs incorporating exact comparisons were made to evaluate vs. compound **15**. Compounds **23** (core III) and **28** (core V) have similar binding activity compared to compound **15**, but compound **33** (core VI) has diminished activity ($K_i = 150$ nM) compared to compound **15**. In the cellular assays, compounds **23** and **28** appear to be slightly more active in the MX-1 proliferation assay, but have somewhat diminished activity in the luciferase reporter assay compared to compound **15**. As seen with the binding assay results, compound **33** is less potent than compound **15** in both the MX-1 proliferation assay and the luciferase reporter assay. Core III does, however, have the advantage with regard to unbound intrinsic clearance in mouse liver microsomes (<7.1 L/hr/kg for compound **23** vs. 55 L/hr/kg for compound **15**). Two additional sulfonyl-containing moieties, ethanesulfonamide (compound **36**) and methylene-linked methylsulfone (compound **40**) were incorporated into compounds of core VII. Both replacements were well-tolerated showing similar or slightly improved activity in the TR-FRET assay compared to the typical methanesulfonamide moiety ($K_i = 11$ nM for compound **36** and $K_i = 11$ nM for compound **40** vs. $K_i = 17$ nM for compound **35**).

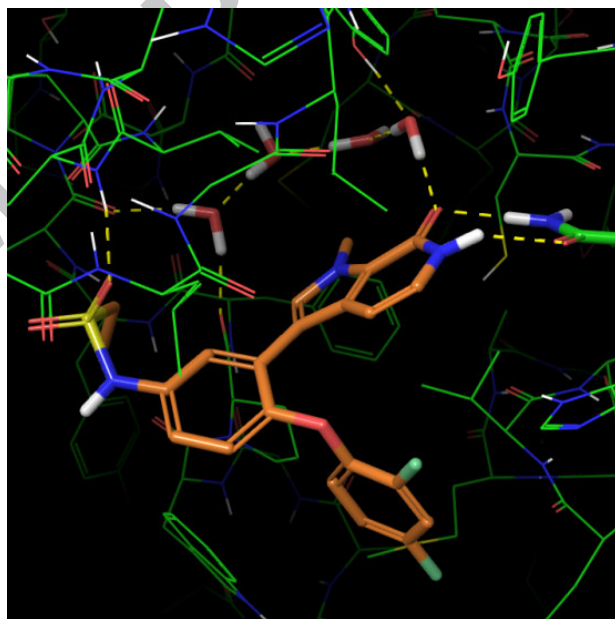


Figure 10. X-ray co-crystal structure of compound **36** in the BRD4 BDII protein. Dotted lines represent H-bonds predicted by Schrödinger Maestro.

Additional X-ray co-crystal structures were obtained to determine whether fully elaborated molecules based on the new cores would bind to the BRD4 BDII protein in the ring flipped conformation observed for the isoindolone ring system of compound **15** or if they would retain the original binding conformation observed for fragment **2**, which would allow a bidentate interaction with ASN433. It can be seen in Figures 10 and 11 that fully elaborated compounds **36** (core VII) (PDB code: 5UEO) and **29** (core V) (PDB code: 5UEQ) both bind to the BRD4 BDII protein with the original conformation observed for fragment **2**, with each making the intended bidentate Asn433 interaction. Among the X-ray co-crystal structures obtained, compound **15** was the only compound for which rotation of the fused bicyclic ring system was observed.

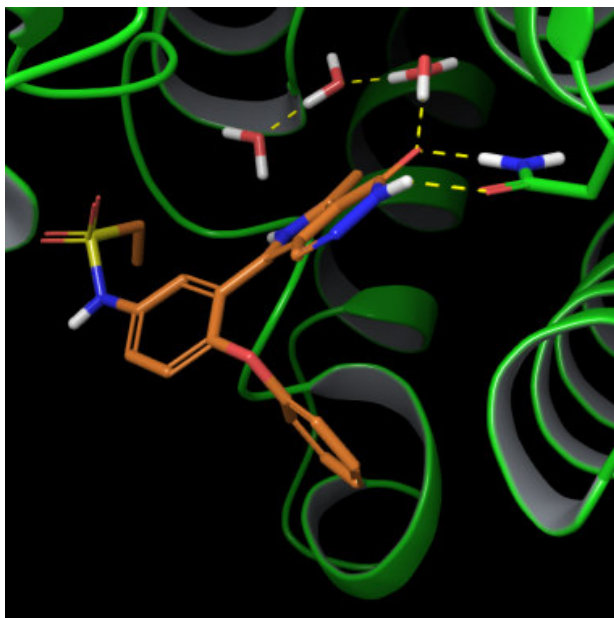


Figure 11. X-ray co-crystal structure of compound **29** in the BRD4 BDII protein. Dotted lines represent H-bonds predicted by Schrödinger Maestro.

Three compounds, **25**, **38** and **39**, were further evaluated in mouse pharmacokinetic studies (Table 4). Although high potency is very desirable, elements such as structural diversity and ADME properties also played a large role in the selection process for pharmacokinetic experiments. Compound **25** is a core III compound with the methylsulfonyl and 2,4-difluorophenyl moieties that exhibited very low unbound intrinsic clearance in mouse liver microsomes and good permeability. Compound **25** demonstrated a 6-fold improvement in both unbound i.v. clearance (14 L/hr/kg vs. 84 L/hr/kg) and unbound oral AUC (0.53 $\mu\text{M}\cdot\text{hr}$ vs. 0.09 $\mu\text{M}\cdot\text{hr}$) compared to compound **15**. However, the oral bioavailability was nearly the same (32% vs. 30%). Compound **38** also incorporates the methylsulfonyl and 2,4-difluorophenyl moieties, but is a core VII compound with greater potency and permeability than compound **25**. It also demonstrated improvements in both unbound i.v. clearance and unbound oral AUC compared to compound **15**, and had nearly double the oral bioavailability (57% vs. 30%). Incorporation of core VII with an ethanesulfonamide moiety and just a single fluoro group at the 4-position of the phenoxy ring in compound **39** resulted in very good potency ($K_i = 5.5$ nM). Unfortunately, this combination resulted in higher unbound i.v. clearance at 130 L/hr/kg and lower unbound oral AUC at 0.06 $\mu\text{M}\cdot\text{hr}$ compared to compounds **15**, **25** and **38**. Blocking both the 2- and 4-positions of the terminal phenoxy ring appears to be necessary to reduce metabolism at that site (compound **39** vs. compound **36**).

Since compounds **38** and **25** both achieved improved drug exposure relative to **15**, they were evaluated in the OPM-2 model (Figure 12). The compounds when dosed QD displayed improved tumor growth inhibition relative to **15** QD (64% and 68%, respectively). Tolerability was viewed as adequate with minimal mean weight loss (1-3%) throughout the study for both treatment groups.

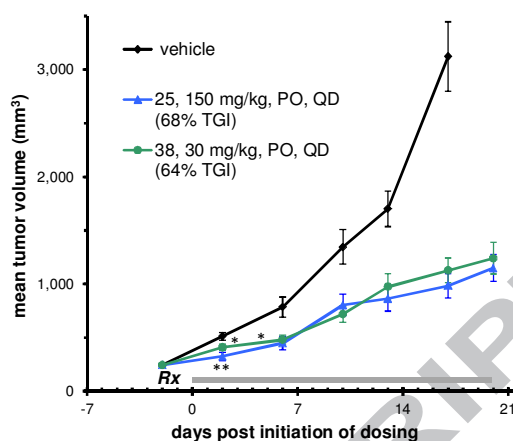


Figure 12. Tumor growth inhibition data for compounds **25** and **38** in an OPM-2 xenograft model of multiple myeloma. Values represent mean \pm SE (n = 10 per group). * indicates animal removed from study.

In summary, the discovery of novel proprietary BET inhibitors was initiated through an NMR fragment screen against BRD4. Two ketopyrrole-based hits **1** and **2** were utilized as the basis for hit-to-lead activities. Structurally-enabled optimization efforts of ketopyrrole fragment **2** to compound **15** improved the TR-FRET activity nearly 760-fold (25 μM vs. 33 nM). Isoindolone **15** exhibited moderate mouse oral bioavailability (30%) and *in vivo* tumor growth inhibition in an OPM-2 xenograft model of multiple myeloma. Further core optimization led to compounds with TR-FRET activity improved in excess of three log units for select examples relative to compound **2**. Gains were also achieved in cellular potency and ADME properties allowing for additional xenograft studies. Compounds **38** and **25** demonstrated tumor growth inhibition of 64% and 68%, respectively, in an OPM-2 model of multiple myeloma which validates pursuit of BET inhibitors as potential cancer therapeutics.

Acknowledgements and Disclosures

This research used resources at the Industrial Macromolecular Crystallography Association Collaborative Access Team (IMCA-CAT) beamline 17-ID, supported by the companies of the Industrial Macromolecular Crystallography Association through a contract with Hauptman-Woodward Medical Research Institute.

This research used resources of the Advanced Photon Source, a U.S. Department of Energy (DOE) Office of Science User Facility operated for the DOE Office of Science by Argonne National Laboratory under Contract No. DE-AC02-06CH11357.

All authors are current or former AbbVie employees. AbbVie was involved in the design, conduct and financial support for this research. AbbVie participated in the interpretation of data, review, and approval of the publication.

Supplementary Material

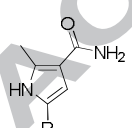
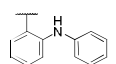
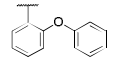
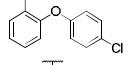
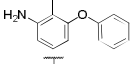
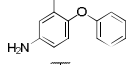
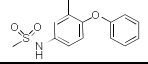
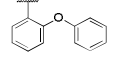
Supplementary data associated with this article can be found, in the online version, at

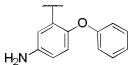
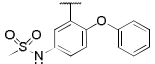
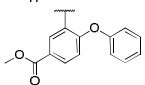
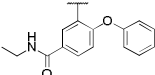
References

- 1) (a) Mujtaba, S.; Zeng, L.; Zhou, M-M. *Oncogene* 2007, 26, 5521. (b) Sanchez, R.; Zhou, M-M. *Curr. Opin. Drug Disc. Dev.* 2009, 12, 659. (c) Shi, J.; Vakoc, C. R. *Mol. Cell* 2014, 54, 728. (d) Fu, L. L.; Tian, M.; Li, X.; Li, J. J.; Huang, J.; Ouyang, I.; Zhang, Y.; Liu, B. *Oncotarget* 2015, 6, 5501.

- 2) (a) Filippakopoulos, P.; Knapp, S. *Nat. Rev. Drug Disc.* **2014**, *13*, 337. (b) Dhalluin, C.; Carlson, J. E.; Zeng, L.; He, C.; Aggarwal, A. K.; Zhou, M.-M. *Nature* **1999**, *399*, 491. (c) Dey, A.; Chitsaz, F.; Abbasi, A.; Misteli, T.; Ozato, K. *Proc. Natl. Acad. Sci. U.S.A.* **2003**, *100*, 8758.
- 3) (a) For a recent Perspectives article on bromodomain inhibitors, see Romero, F. A.; Taylor, A. M.; Crawford, T. D.; Tsui, V.; Cote, A.; Magnuson, S. *J. Med. Chem.* **2016**, *59*, 1271. (b) For a recent review on the clinical development of BET bromodomain inhibitors, see Theodoulou, N. H.; Tomkinson, N. C. O.; Prinjha, R. K.; Humphreys, P. G. *Curr. Opin. Chem. Biol.* **2016**, *33*, 58.
- 4) Shuker, S. B.; Hajduk, P. J.; Meadows, R. P.; Fesik, S. W. *Science* **1996**, *274*, 1531.
- 5) (a) For information on an additional core we identified through the NMR fragment screen, see Wang, L.; Pratt, J. K.; Soltwedel, T.; Sheppard, G. S.; Fidanze, S.; Liu, D.; Hasvold, L. A.; Mantei, R. A.; Holms, J.; McClellan, W.; Wendt, M.; Wada, C.; Frey, R.; Hansen, T. M.; Hubbard, R.; Park, C.; Li, L.; Magoc, T.; Albert, D. H.; Lin, X.; Warder, S. E.; Kovar, P.; Huang, X.; Wilcox, D.; Wang, R.; Rajaraman, G.; Petros, A.; Hutchins, C.; Torrent, M.; Panchal, S. C.; Sun, C.; Elmore, S. W.; Rosenberg, S.; Shen, Y.; McDaniel, K. F.; Kati, W. Manuscript in preparation. (b) Subsequent to our discovery and submission of a patent application, another group independently reported the discovery of 3-keto-2-methylpyrrole binders of BET-bromodomains through a virtual library screen. Lucas, X.; Wohlwend, D.; Hügler, M.; Schmidtkunz, K.; Gerhardt, S.; Schüle, R.; Jung, M.; Einsle, O.; Günther, S. *Angew. Chem. Int. Ed.* **2013**, *52*, 14055. (c) Recently another group independently reported the discovery of bromodomain scaffolds through the use of biosensor fragment screening. Navratilova, I.; Aristotelous, T.; Picaud, S.; Chaikuad, A.; Knapp, S.; Filippakopoulos, P.; Hopkins, A. L. *ACS Med. Chem. Lett.* **2016**, *7*, 1213.
- 6) Abad-Zapatero, C.; Metz, J. T. *Drug Discovery Today* **2005**, *10*, 464.
- 7) Dhalluin, C.; Carlson, J. E.; Zeng, L.; He, C.; Aggarwal, A. K.; Zhou, M.-M. *Nature* **1999**, *399*, 491.
- 8) Mitsubishi Tanabe Pharma Corporation WO 2009/2009084693.
- 9) Nicodeme, E.; Jeffrey, K. L.; Schaefer, U.; Beinke, S.; Dewell, S.; Chung, C.-W.; Chandwani, R.; Marazzi, I.; Wilson, P.; Coste, H.; White, J.; Kirilovsky, J.; Rice, C. M.; Lora, J. M.; Prinjha, R. K.; Lee, K.; Tarakhovskiy, A. *Nature* **2010**, *468*, 1119.
- 10) (a) Filippakopoulos, P.; Knapp, S. *FEBS Lett.* **2012**, *586*, 2692. (b) Filippakopoulos, P.; Picaud, S.; Mangos, M.; Keates, T.; Lambert, J.-P.; Barsyte-Lovejoy, D.; Felletar, I.; Volkmer, R.; Müller, S.; Pawson, T.; Gingras, A.-C.; Arrowsmith, C. H.; Knapp, S. *Cell* **2012**, *149*, 214.
- 11) Smith, J. A.; White, E. A.; Sowa, M. E.; Powell, M. L. C.; Ottinger, M.; Harper, J. W.; Howley, P. M. *Proc. Natl. Acad. Sci. U.S.A.* **2010**, *107*, 3752.
- 12) Clezy, P. S.; Fookes, C. J. R.; Mirza, A. H. *Aust. J. Chem.* **1977**, *30*, 1337.
- 13) Bheeter, C. B.; Bera, J. K.; Doucet, H. *Tetrahedron Lett.* **2012**, *53*, 509.

Table 1. SAR of fragment analogs.

Core	ID	R	TR-FRET K_i (nM)	MX-1 Proliferation EC_{50} (nM)	Luciferase Reporter (10% FBS) EC_{50} (nM)
	4		22,000	>10,000	>10,000
	7		450	6,900	2,800
	8		270	970	450
	9		410	1,200	280
	10		1,600	>3,000	2,100
	11		420	690	880
	12		280	1,000	1,400
	5		9,500	>10,000	7,100
	13		440	1,400	280

14		210	230	300
15		33	160	51
16		91	1,200	2,000
17		250	1,400	1,400

TR-FRET BRD4 K_i values are reported as the geometric mean derived from 2 or more measurements. running MSR = 1.2 and test-retest MSR = 2.1.
 EC_{50} values are reported as the mean derived from two measurements.

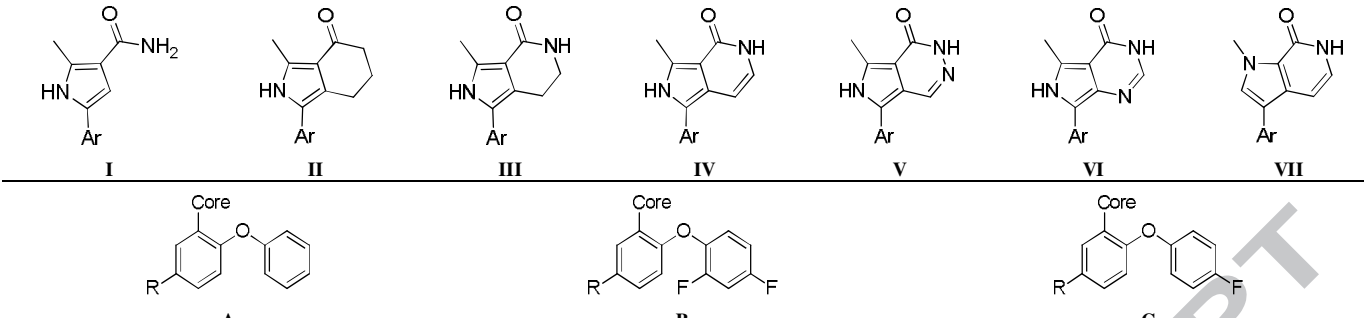
MX-1 proliferation assay: running MSR = 1.2 and test-retest MSR = 4.7.

Luciferase reporter assay: running MSR = 1.3 and test-retest MSR = 2.6.

Table 2. Mouse PK of compound 15.

ID	I.V. unbound CLP (L/hr/kg)	P.O. unbound AUC ($\mu\text{M}\cdot\text{hr}$)	I.V. $t_{1/2}$ (hr)	F (%)
15	84	0.09	0.6	30

I.V. dose: 3 mg/kg; P.O. dose: 10 mg/kg.

Table 3. Data comparison of cores I-VII.


The figure shows the chemical structures of seven different cores (I-VII) and their substituents A, B, and C. Cores I-VII are shown as fused ring systems with an NH group and an Ar group. Substituents A, B, and C are shown as phenyl rings with various functional groups (R, H, NHSO₂Me, SO₂Me, F).

Core	ID	R	Ar	TR-FRET K _i (nM)	MX-1 EC ₅₀ (nM)	Reporter 10% FBS EC ₅₀ (nM)	Clint, u Mouse (L/hr/kg)	Permeability (x10 ⁶ cm/s)
I	8	H	A	270	970	450	540	29
	12	NHSO ₂ Me	A	280	1,000	1,400	21	12
	18	NHSO ₂ Me	B	370	660	2,300	8.1	NA
	19	SO ₂ Me	B	2,200	3,200	4,500	6.0	NA
II	13	H	A	440	1,400	280	10,000	9.5
	15	NHSO ₂ Me	A	33	160	51	55	27
	20	NHSO ₂ Me	B	97	250	75	49	19
	21	SO ₂ Me	B	460	570	1,400	84	NA
III	22	H	A	340	190	280	NA	NA
	23	NHSO ₂ Me	A	41	55	120	<7.1	15
	24	NHSO ₂ Me	B	84	230	420	19	8.7
	25	SO ₂ Me	B	300	900	290	<6.9	22
IV	26	H	A	450	220	700	1,900	61
	27	H	A	37	180	220	520	30
	28	NHSO ₂ Me	A	30	59	180	37	10
	29	NHSO ₂ Et	A	10	52	75	48	9.5
	30	NHSO ₂ Me	B	16	92	280	>15	6.1
V	31	SO ₂ Me	B	77	390	750	37	12
	32	H	A	1,100	1,200	1,600	>370	100
	33	NHSO ₂ Me	A	150	460	410	36	13
VII	34	H	A	120	580	1,100	6,400	13
	35	NHSO ₂ Me	B	17	38	46	29	21
	36	NHSO ₂ Et	B	11	56	56	12	14
	37	SO ₂ Me	A	17	68	91	22	48
	38	SO ₂ Me	B	98	110	150	12	35
	39	NHSO ₂ Et	C	5.5	21	47	20	32
	40	CH ₂ SO ₂ Me	B	11	20	40	24	40

TR-FRET BRD4 K_i values are reported as the geometric mean derived from 2 or more measurements: running MSR = 1.2 and test-retest MSR = 2.1.

EC₅₀ values are reported as the mean derived from two measurements.

MX-1 proliferation assay: running MSR = 1.2 and test-retest MSR = 4.7.

Luciferase reporter assay: running MSR = 1.3 and test-retest MSR = 2.6.

Clint, u mouse: scaled unbound intrinsic clearance in mouse liver microsomes.

Table 4. Mouse PK data for select compounds.

ID	I.V. unbound CL _p (L/hr/kg)	P.O. unbound AUC (μM*hr)	I.V. t _{1/2} (hr)	F (%)
15	84	0.09	0.6	30
25	14	0.53	1.3	32
38	16	0.86	2.5	57
39	130	0.06	5.6	33

I.V. dose: 3 mg/kg; P.O. dose: 10 mg/kg.

ACCEPTED MANUSCRIPT